A novel approach to flow estimation in tidal rivers

H. R. Moftakhari,[1] D. A. Jay,[1] S. A. Talke,[1] T. Kukulka,[2] and P. D. Bromirski[3]

Received 7 September 2012; revised 7 June 2013; accepted 13 June 2013; published 7 August 2013.

[1] Reliable estimation of river discharge to the ocean from large tidal rivers is vital for water resources management and climate analyses. Due to the difficulties inherent in measuring tidal-river discharge, flow records are often limited in length and/or quality and tidal records often predate discharge records. Tidal theory indicates that tides and river discharge interact through quadratic bed friction, which diminishes and distorts the tidal wave as discharge increases. We use this phenomenon to develop a method of estimating river discharge for time periods with tidal data but no flow record. Employing sequential 32 day harmonic analyses of tidal properties, we calibrate San Francisco (SF), CA tide data to the Sacramento River delta outflow index from 1930 to 1990, and use the resulting relationship to hindcast river flow from 1858 to 1929. The M_2 admittance (a ratio of the observed M_2 tidal constituent to its astronomical forcing) best reproduces high flows, while low-flow periods are better represented by amplitude ratios based on higher harmonics (e.g.,M_4/M_2^2). Results show that the annual inflow to SF Bay is now 30% less than before 1900 and confirm that the flood of January 1862 was the largest since 1858.

Citation: Moftakhari, H. R., D. A. Jay, S. A. Talke, T. Kukulka, and P. D. Bromirski (2013), A novel approach to flow estimation in tidal rivers, *Water Resour. Res.*, *49*, 4817–4832, doi:10.1002/wrcr.20363.

1. Introduction

[2] Accurate freshwater discharge estimates for rivers that interact with ocean tides are needed for many purposes, e.g., flood management and reservoir operations [*Madsen and Skotner*, 2005; *Kisi and Cimen*, 2011; *Wang et al*., 2009]. The discharge of large tidal rivers to the ocean is an important component of the global water balance [*Oki et al*., 1995], and changes in discharge affect sediment input to the ocean [*Syvitski et al*., 2003]. Both are important for climate analyses [*Laize and Hannah*, 2010] and water resources management [*Loitzenbauer and Mendes*, 2012]. On a smaller scale, accurate river discharge measurements are required to assess coastal inundation and plan navigation projects [*Peng et al*., 2004; *Prandle*, 2000], as well as for analyses of coastal upwelling [*Gan et al*., 2009; *Palma et al*., 2006], beach sediment supply [*Flick and Ewing*, 2009; *Inman and Jenkins*, 1999], estuarine sediment supply and transport [*Jay et al*., 1990; *Prandle*, 2004; *Schoellhamer et al*., 2007; *Ganju et al*. 2008], habitat access and restoration [*Kimmerer*, 2002; *Kukulka and Jay*, 2003a, 2003b; *Cloern et al*., 1983], salinity intrusion [*Prandle*, 1985; *Uncles and Peterson*, 1996; *Cloern et al*., 1989; *Monismith et al*., 2002], and impacts of future climate change [*Kukulka and Jay*, 2003a, 2003b].

[3] The lower reach of a tidal river is, however, a difficult location to determine net flow for methodological reasons. Difficulties include the reversing tidal flow, the compensation flow for the tidal Stokes drift, spring-neap water storage effects, lateral circulation, and the presence in some systems of multiple distributaries or separate ebb/flood channels. Recent studies have introduced methods to calculate discharge in tidal rivers. While these studies were suited for cases far from the mouth [*Hoitink et al*., 2009; *Sassi et al*., 2011a; *Kawanisi et al*., 2010], it remains very difficult to determine a statistically significant discharge near the mouth of an estuary [*Jay et al*., 1997]. Thus, discharge gauging stations are typically located above the head of the tide, often hundreds of kilometers inland. At those locations, infiltration and inflows from coastal tributaries in areas of high precipitation and downstream losses from diversion and evaporation are not included in the measured flow.

[4] The purpose of this paper is to demonstrate the feasibility and utility of a tidal discharge estimate (TDE) based on analysis of tidal statistics, using known astronomical forcing. The physical basis of the TDE is that nonlinear bed friction couples tides and river discharge (Figure 1) in a manner that can be modeled analytically [c.f., *Godin*, 1999; *Jay*, 1991]. If discharge and astronomical (or coastal) tidal forcing are known, the tidal response may be predicted by a forward model [*Jay and Flinchem*, 1997; *Kukulka and Jay*, 2003a, 2003b]. Conversely, if observed tides and the astronomical or coastal forcing are known,

Additional supporting information may be found in the online version of this article.

[1]Department of Civil and Environmental Engineering, Portland State University, Portland, Oregon, USA.
[2]College of Earth, Ocean, and Environment, University of Delaware, Newark, Delaware, USA.
[3]Scripps Institution of Oceanography, University of California, San Diego, La Jolla, California, USA.

Corresponding author: H. R. Moftakhari, Department of Civil and Environmental Engineering, Portland State University, PO Box 751, Portland, OR 97207-0751, USA. (hamed2@cecs.pdx.edu)

0043-1397/13/10.1002/wrcr.20363

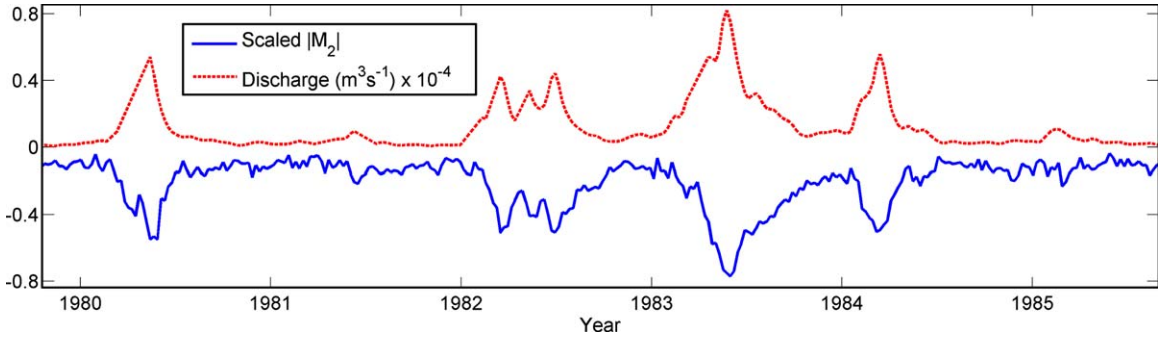

Figure 1. Example of the interaction of tides with river flow in the San Francisco Bay; $|M_2|$ has been scaled relative to the difference between the minimum and maximum M_2 (change in $|M_2|$/[maximum change in $|M_2|$]); flow is the NDOI. The mean $|M_2|$ amplitude is 0.57 m, while the maximum change in $|M_2|$ is ∼0.12 m.

discharge may be estimated via an inverse model. While TDE has been outlined [*Jay and Kukulka*, 2003] and tested in a preliminary way [*Jay et al*., 2005], this contribution represents the first detailed test of the method, including a quantification of uncertainties. To test and demonstrate the TDE, an inflow record for the San Francisco (SF) Bay, CA is constructed for the 1858–2010 period.

[5] The SF Bay delta, through which most freshwater reaches the bay, is a good example of the difficulties inherent in flow estimates for tidal rivers. Uncertainty in the timing and magnitude of freshwater inflow into the bay exists because the delta is a network of channels with numerous connections, diversions, inputs, and outputs [*Kimmerer*, 2002]. Also, estimates of groundwater recharge and losses from diversion, evaporation, and infiltration are included in the flow index used to estimate flows into the bay (http://www.water.ca.gov/dayflow/output/) and may not always be available or accurate. While for many purposes the estimation of discharge to the ocean is desired, conditions at the ocean boundary are not conducive to long-term flow measurements. Decades of experience in estuarine flux measurement has established that net, nontidal fluxes of water usually cannot be measured in estuaries, because they are small relative to tidal fluxes [*Jay et al*., 1997]; however, subtidal estuarine exchange flow can be estimated using numerical methods [*MacCready*, 2011].

[6] One advantage of using TDE in SF Bay is that it moves the nexus of measurement away from the complexities of the delta, without requiring flux measurements at the ocean entrance. Because tide gauges are needed for safe navigation and tidal prediction, they were often installed well before the onset of systematic river gauging [*Talke and Jay*, 2013], providing an opportunity to extend flow records back in time using TDE. Continuous tide measurements began in 1853 in the Eastern Pacific and in 1858 in the Western Pacific [*Talke and Jay*, 2013], and a tide gauge has operated continuously in SF, since 1854 [*Smith*, 2002]. The hourly record has been digitized and is described in *Bromirski et al*. [2003]. While some stage measurements exist for the Sacramento River from as early as 1850 [*Logan*, 1864], subsequent levee construction and sedimentation due to hydraulic mining make early measurements difficult to interpret [*Gilbert*, 1917]. As a consequence, commonly accepted estimates of Sacramento Delta river-flow begin in 1930, with the California Department of Water Resources' Net Delta Outflow Index (NDOI) (www.water.ca.gov/dayflow/output/). Earlier flow measurements are available (e.g., daily flow at Red Bluff from 1891), but are far from the Golden Gate and do not adequately represent basin-scale processes. To avoid these problems, earlier studies have used precipitation data to estimate pre-1930 hydrographs of flow from the watershed to the estuary [e.g., *Ganju et al*., 2008]. However, such methods cannot easily take into account natural and anthropogenic changes to the system, including changing snow levels and snowmelt patterns, the channelization of river flow and the subsequent reduction in flood-plain area, and the effects of reservoir management. We argue that for estimating net flow from the estuary to the ocean, such problems can be reduced or eliminated by application of TDE to historic tide data at a location (e.g., the Golden Gate) which is much less altered than inland locations, and which integrates processes over a basin scale. TDE may therefore capture changes in reservoir management, climate cycles, and long-term hydrological trends that cannot easily be ascertained from other data sources.

2. Data and Methods

2.1. Setting

[7] The SF Bay consists of two distinct subestuaries. The northern reach, the SF Bay delta, is a partially mixed estuary dominated by seasonally varying fresh water inflows, while the southern part is a tidal lagoon estuary and typically well mixed [*Cheng and Gartner*, 1985; *Chua and Fringer*, 2011]. Freshwater inflow occurs primarily from the Sacramento and San Joaquin Rivers (Figure 2), with annual average flows of 558 and 126 $m^3\ s^{-1}$, respectively (http://wdr.water.usgs.gov/). Flows in both systems have been reduced and altered considerably by diversion [*Kimmerer*, 2002]. The tides in SF Bay have a mixed diurnal-semidiurnal character. Analyses (below) of data from the SF tide gauge at the Presidio (Figure 2) show that the present amplitude of the major semidiurnal constituent M_2 is 0.57 m, while the largest diurnal K_1 constituent has an amplitude of 0.37 m. The M_2 and K_1 amplitudes in SF Bay have increased since 1854, with the change in M_2 (0.4 mm yr^{-1} or 7% $century^{-1}$) being particularly prominent

Figure 2. San Francisco Bay delta watershed boundaries and tributaries (USGS, HUC (Hydrologic Unit Code), http://www.nationalatlas.gov/); points A, B, C, and D show tide gage locations (NOAA Station ID: 9414290) at Fort Point (1854–1877), Sausalito (1877–1897), Presidio (1897–1927), and Presidio (1927–present), respectively. The red circle shows the stream gauge site for Sacramento River near Red Bluff (USGS 11377100); the red triangle indicates the Shasta Dam (©ESRI).

[*Jay*, 2009]. These factors must be taken into account in our analyses.

2.2. Data Sources

2.2.1. Tide Data

[8] Hourly SF water level data from the National Oceanic and Atmospheric Administration (NOAA; station ID: 9414290) were used to implement TDE in SF Bay. This station has the longest continuous tidal record in the United States, but has been located in at least seven places since its installation in 1854. It is now located on southern side of the bay entrance channel (the "Golden Gate"), at 37°48.4′N and 122°27.9′W (Figure 2). The gauge was first installed 640 m east of Fort Point on 30 June 1854 [*Smith*, 2002]. In 1877, decay of the Fort Point wharf necessitated moving the gauge. It was relocated to Sausalito, 3.2 km to the north and further from the entrance, from 1877 to 1897. In 1897, the gauge was moved back across the Golden Gate to the Presidio, about 1.2 km east of Fort Point. In 1927, it was moved to its present location at the Fort Point Coast Guard wharf at Crissy Field [*Smith*, 2002], 1.55 km east of Fort Point. Although the official NOAA history [*Smith*, 2002] does not indicate this, our examination of the marigrams that serve as the basis for the hourly record indicates that the gauge was moved at least once in 1862 and perhaps more than once, due to damage caused by the extraordinary storms of that winter. Due to subsidence, the gauge was also moved in April 1858 and again in July 1859 to new locations adjacent to the original Fort Point wharf [see also *Talke and Jay*, 2013]. Before April 1858, comparisons show that the self-recording gauge was erratic, with water level errors of up to 0.5 m relative to a fixed staff during some months [*Talke and Jay*, 2013]. Combined with the subsidence issue, the data until early 1858 are considered unreliable and are not used here [see also *Bromirski et al*., 2003]. Nonetheless, the overall gauge record is relatively complete, with only ∼7838 hourly data missing in the 157 year length of record.

2.2.2. Discharge and Precipitation Data

[9] In this study, we use the NDOI, an output of the California Department of Water Resources DAYFLOW program (http://www.water.ca.gov/dayflow/), as a proxy for tidally average daily river inflow to SF Bay from the Sacramento River delta. NDOI accounts for about 90% of the inflow to SF Bay; about 10% comes from local tributaries [*Conomos and Peterson*, 1977]. NDOI accounts for river inflows, precipitation, agricultural consumptive demand, and California Water Project exports. Sixty-one years of NDOI measurements (from 1930 to 1990) are used to calibrate our TDE model, and 20 years (1991–2010) are used to validate it. Because fewer stream gauge sites were in place before 1956, NDOI estimates for 1930–1955 are less certain than those for later periods (D. Schoellhamer, personal communication, USGS, Sacramento, CA). Also, NDOI does not account for tidal monthly increases in storage during periods of larger tides, an effect that is likely to be largest during low-flow periods.

[10] We also use the daily discharge measured at Red Bluff, CA (USGS 11377100) from 1891-present, to check the accuracy of the model. For comparison with tidal properties, which are harmonically analyzed over 32 day window (see section 2.3.2), the daily discharge data were sampled with a 32 day moving average, calculated at 7 day intervals. Data were weighted with a Kaiser filter [*Kaiser*, 1974] with a side lobe attenuation factor of 4.5.

[11] Our estimates of inflow to SF Bay are also compared to two measures of unimpaired flow to the bay. The Eight-River Index (ERI), published by The California Department of Water Resources (http://cdec.water.ca.gov/), combines the flows into the Sacramento and San Joaquin Rivers from major tributaries, including the Feather, Yuba, American, Stanislaus, Tuolomne, and Merced Rivers, after removing the effect of diversions, storage, export, and import. It is available as monthly totals for the wet half of the water year (December–May) back to 1906 [*Ganju et al*., 2008]. The ERI provides a valuable check to pre-1930 hindcasts. The post-1930 ERI is useful for investigating the effect of water resources management measures.

[12] Finally, TDE hindcasts were compared to precipitation data from SF (1850–present) provided by Golden Gate Weather Services (http://ggweather.com/sf/monthly.html).

2.3. Methods

2.3.1. Conceptual Basis

[13] Observed tides are the result of astronomical forcing and propagation/damping in the ocean and coastal waters. At open-ocean locations, tides can be approximately described in terms of five primary astronomical constituents (M_2, S_2, N_2, K_1, and O_1) and several hundred smaller ones [*Parker*, 2007]. In estuaries and shallow water, however, nonlinear terms in the long-wave equations that describe tidal motion can significantly modify wave propagation and amplitude, adding many "shallow water" or "overtide" constituents at multiples or sums of the basic astronomical tidal frequencies [*Doodson*, 1957; *LeBlond*, 1978]. The most important nonlinearity in tidal rivers is quadratic bed-stress, $\tau_B = \rho C_D |U| U$, which alters wave amplitude and phase and exchanges energy between frequencies [*Parker*, 1991]. Here ρ is water density; U is dimensional total velocity, the sum of river flow plus tidal flow; and C_D is the drag coefficient. If the fluvial velocity is a significant fraction of the tidal current amplitude, the absolute velocity in τ_B is a nonlinearity that complicates analytical manipulation—the flow reverses, but not for half of the tidal cycle. This motivates expression of τ_B using a Tschebyshev expansion [*Dronkers*, 1964]:

$$\frac{\tau_B}{\rho} = C_D|U|U \approx C_D U_0^2 \Big[a_1(U_T + U_R) + a_2(U_T + U_R)^2 + a_3(U_T + U_R)^3\Big] \tag{1}$$

where a_i are coefficients that depend on ratio of river flow to total flow, U_0 is a velocity scale, U_R (<0; i.e., flowing seaward) is nondimensional river flow (sum of all flows at subtidal frequencies), and U_T is nondimensional total tidal velocity (sum of flow for all tidal frequencies); all variables are sectionally averaged. To determine how tidal properties will vary with flow, equation (1) must still be embedded in a one-dimensional analysis of the wave equation in such a way that the influence of changes in flow can be traced.

[14] *Kukulka and Jay* [2003a, 2003b] carried out such an analysis, assuming strong bed friction; time-invariant, exponential channel geometry; a single source of river flow far upriver; and negligible influence from wind stress and baroclinic forcing. They then employed a perturbation method to obtain the lowest order wave equation (see *Kukulka and Jay* [2003a, 2003b] for more details). In the case of high-river flow ($|U_R| \approx |U_T|$), and taking only the component at the frequency of U_T, a_1 and a_3 are $\sim$0, as expected from the quadratic drag law [*Kukulka and Jay*, 2003a, 2003b]. Thus, equation (1) reduces to:

$$\frac{\tau_B}{\rho} \approx 2C_D U_0^2 a_2 U_T U_R = -2C_D U_0^2 U_T |U_R| \qquad a_2 \approx 1 \quad (2a)$$

[15] As suggested by equation (2a) and Figure 1, an increase in discharge amplitude $|U_R|$ increases τ_B and damps the tide. Tidal phase is also modified, because the ratio of the acceleration and friction in the wave equation is altered [*Godin*, 1985, 1999; *Jay and Flinchem*, 1997; *Kukulka and Jay*, 2003a; *Buschman et al*., 2009]. This damping of river tides suggests that it can be used to estimate river flow via an inverse model, at least for high flows. (More generally, C_D in equation (1) may also be modified, due to changes in salinity intrusion and/or bedform characteristics. This does not affect the applicability of TDE, as long as the product $C_D|U_R|$ varies in a consistent manner with flow, though it may influence the parameterization used for TDE.)

[16] Damping of the tide as suggested by equation (1) is only one possible type of tidal-fluvial interaction. Nonlinear friction also distorts the tide as it propagates, and appears in the tidal record as nonlinear "overtides," or higher harmonics of combinations of primary constituents [*Parker*, 2007]. For example, self-interaction of M_2, a quadratic nonlinearity that rises rapidly in importance as river flow increases, generates the overtide M_4, with half the period of M_2. This possibility can be seen by rephrasing equation (1) for low river flow:

$$\frac{\tau_B}{\rho} \approx 2C_D U_0^2 \left[a_1 U_T + a_3 \left(U_T^3 + 3U_R U_T^2\right)\right] \qquad (2b)$$

where $a_2 \sim 0$ for low flows [*Kukulka and Jay*, 2003a, 2003b]. While the cubic term in equation (2b) contains a mix of tidal and overtide terms, the overtide term containing ${U_T}^2$ is proportional to U_R. We conclude from these asymptotic forms that frictional damping of the tides is quantitatively related to river flow, but that multiple mechanisms are present. Thus, there may be more than one tidal statistic that can be used to infer flow from tidal properties.

[17] The bottom stress parameterizations, equations (1) and (2), reveal the interaction of tides with river flow and can be incorporated in a cross sectionally averaged tidal propagation model. In such a model, tidal wave propagation is described by a complex wave number $q = k + ir$ that is the eigenvalue of the wave equation. Here $k = 2\pi/\lambda > 0$ (λ is wavelength), and $r < 0$ is the damping modulus. Based on tidal theory [*Jay*, 1991], wave amplitude and r can be approximated [*Kukulka and Jay*, 2003a] at any distance from the ocean x:

$$\frac{|\mathrm{TP}_X|}{|\mathrm{TP}_{\mathrm{ref}}|} = e^{-rx} \qquad (3a)$$

$$-rx \approx \log\left(\frac{|\mathrm{TP}_X|}{|\mathrm{TP}_{\mathrm{ref}}|}\right) \cong c_0' + c_{1a}' U_R^{\frac{1}{2}} + c_{1b}' U_R^{\frac{3}{2}} + c_2' \frac{U_T^2}{\sqrt{U_R}} \qquad (3b)$$

$$r \approx c_0 + c_1 U_R^n + c_2 \frac{T_{R\mathrm{ref}}^2}{\sqrt{U_R}} \qquad 0.5 \le n \le 1.5 \qquad (3c)$$

where $\mathrm{TP}_{\mathrm{ref}}$ is a reference tidal property (amplitude or range) in the astronomical potential or at a coastal reference station removed from the influence of river flow, TP_X is a tidal property at point x, x is taken as constant (and absorbed into the c_i), and $T_{R\mathrm{ref}}$ is tidal range at the reference station. Parameters c_i and c_i' vary with x, channel shape and U_R/U_T, and equation (3c) is a pragmatic simplification that reduces the number of free parameters. The last term in equation (3c) represents a tidal monthly modulation of tidal properties, the amplitude of which is dependent on the inverse square root of the river flow. Equation (3c) with $n = 1$ is the basis of the forward model used by *Kukulka and Jay* [2003a] and *Jay et al*. [2011] for hindcasts of tidal properties.

[18] The relative importance of the terms in equation (3c) depends on the characteristic s of the system. Preliminary analyses showed that in SF Bay, tidal range deviates <20% from its monthly mean over a typical month, and these deviations are largely averaged out over the 31.7d analysis period used here. The last term in equation (3c) is therefore much smaller than the second term, which can vary by several orders of magnitude over a year. Thus, the last term has been neglected in our TDE inverse model. A further simplification is achieved using a Taylor expansion of $\log(\mathrm{TP}_X/\mathrm{TP}_{\mathrm{ref}})$, recognizing that $\mathrm{TP}_X/\mathrm{TP}_{\mathrm{ref}} \approx 1$:

$$\log\left(\frac{\mathrm{TP}_X}{\mathrm{TP}_{\mathrm{ref}}}\right) = \log(1-\delta) = \delta + \ldots \approx \delta$$
$$\delta = \frac{\mathrm{TP}_{\mathrm{ref}} - \mathrm{TP}_X}{\mathrm{TP}_{\mathrm{ref}}} << 1 \qquad (4)$$

where higher terms are neglected, and "log" is the natural logarithm.

[19] Together equations (1)–(4) suggest a relationship between the monthly averages of a tidal property ratio ($\mathrm{TP}_R = \mathrm{TP}_X/\mathrm{TP}_{\mathrm{ref}}$) and U_R of the form:

$$\mathrm{TP}_R \approx \alpha_1 + \beta_1 U_R^{n_1} \qquad (5)$$

where α_1, β_1, and n_1 are coefficients to be determined from data, and $0.5 \le n_1 \le 1.5$. Assuming a constant (over a tidal cycle) cross-sectional area A, U_R can be replaced by river discharge ($Q_R \cong A \times U_R$):

$$\mathrm{TP}_R \approx \alpha_2 + \beta_2 Q_R^{n_1} \qquad (6)$$

[20] Equation (6) is perhaps the simplest form of a forward model for determining tidal properties (averaged over a tidal month), given astronomical or coastal tidal forcing and river flow. To obtain Q_R from known tidal properties, TDE inverts equation (6) to reach a binomial form, while the fact that n_1 is $O(1)$ allows truncation of the power series to two terms:

$$Q_R \approx \alpha + \beta \mathrm{TP}_R{}^{\gamma} \quad \text{where } \frac{2}{3} \le \gamma \le 2. \qquad (7)$$

2.3.2. Tidal Estimates

[21] Application of TDE based on equation (7) requires that tidal properties be determined as a time series with a resolution of a few days to weeks. One way to do this is through use of overlapping, short harmonic analyses. A harmonic analysis (HA) provides a least-squares fit description of the changing elevation of the sea surface at a point as a sum of a finite number of sine and cosine waves of known frequency; the amplitudes and phases are the parameters determined by a least-squares fit [*Parker*, 2007]. The tidal analysis program T_Tide [*Pawlowicz et al*., 2002] is used here, in a modified form that employs a robust least-squares solution to determine the tidal parameters [*Leffler and Jay*, 2009].

[22] Defining an analysis window length is an important concern in analysis of nonstationary data. Short HA analysis windows (<15d) cause mixing of information between tidal frequencies [*Jay and Flinchem*, 1999], whereas long tidal windows will average out flow variability. In this study, sequential 761h (31.7d) harmonic analyses were carried out at 7d intervals over the length of record, with 59 constituents included in the analysis. Only data that were >80% complete over a 761h increment were analyzed.

[23] A 31.7d analysis window is long relative to river flow fluctuations associated with winter floods, and use of a normal 31.7d HA analysis window (which is effectively a boxcar filter) causes considerable averaging of flow-affected tidal properties and may, like any short harmonic analysis, report tidal properties that reflect some degree of aliasing [*Jay and Flinchem*, 1999]. To minimize these problems, the HA was implemented with a Kaiser filter window [*Kaiser*, 1974] with a side lobe attenuation factor of 4.5, rather than the boxcar window that is standard in T_Tide. The Kaiser filter allows for an effective tidal analysis and better resolution of intermittent flood events, while avoiding aliasing [*Jay and Flinchem*, 1999]. More than 80% of the data set energy is within the center 18 days; we therefore assign an effective resolution of 18 days to our analysis.

[24] *Kukulka and Jay* [2003a, 2003b] implement equation (3c) to determine tidal properties (amplitudes, phases, and daily tidal ranges) between a station of interest and a coastal reference station. Because there was only one tide station in SF Bay until recent decades, we use the astronomical tidal potential V (defined in the next paragraph) instead of a coastal reference station. More specifically, we apply equation (7) with $\mathrm{TP}_R = \mathrm{M}_2$ admittance (AD_{M_2}, the ratio of observed to potential M_2) to hindcast moderate and high-flow conditions, as suggested by equation (2a). Low-flow conditions are hindcast using a ratio involving the M_4 overtide in equation (7), as suggested by equation (2b).

[25] The tidal potential V (in $\mathrm{m^2 s^{-2}}$) describes the effect of gravitational acceleration vector (A) from the sun and moon in the form of a gradient [*Pawlowicz et al*., 2002]:

$$A = -\nabla V \tag{8}$$

[26] The ratio V/g has units of m (g is gravitational acceleration in $\mathrm{ms^{-2}}$) and represents the tide that would occur if the ocean were in a frictionless equilibrium with gravitational forcing. Hourly values of V are calculated using a program provided (R. Ray, personal communication) by the National Astronautics and Space Administration (NASA) that is based on *Cartwright and Eden* [1973]. In the Cartwright and Eden approach, V contains ~480 frequencies in diurnal, semidiurnal, terdiurnal (thrice daily), and low-frequency bands. There is no significant astronomical forcing in the quarterdiurnal band (4× daily). Thus, the observed M_4 tide arises entirely from nonlinear processes.

[27] T_Tide was used to calculate amplitudes, phases, and error estimates at 7d intervals for tidal constituents (here M_2 and M_4) for both the observed tidal records and for the hourly time series of V. M_2 admittance is expressed as:

$$\mathrm{AD}_{M_2} = \frac{A_{M_2} e^{i\theta_{M_2}}}{\hat{A} e^{i\hat{\theta}}} \tag{9}$$

where A_{M_2} and θ_{M_2} are, respectively, the amplitude and phase of observed M_2, and $\hat{A}$ and $\hat{\theta}$ are with the same parameters for potential V. The M_2 admittance amplitude ($|\mathrm{AD}_{M_2}|$), will vary with flow, because the observed tide is influenced by flow.

[28] M_4 arises from M_2 via a quadratic nonlinearity and has no astronomical component. Thus, M_4 admittance cannot be defined in the same way as $|\mathrm{AD}_{M_2}|$. We use, therefore, M_2 observations as the reference wave for M_4 and calculate an amplitude ratio and a phase difference as follows:

$$\frac{M_4}{M_2^2} = \frac{A_{M_4} e^{i\theta_{M_4}}}{A_{M_2}^2 e^{2i\theta_{M_2}}} \Rightarrow A_{\frac{M_4}{M_2^2}} = \frac{A_{M_4}}{A_{M_2}^2}, \qquad \theta_{\frac{M_4}{M_2^2}} = \theta_{M_4} - 2\theta_{M_2} \tag{10}$$

2.3.3. Detrending

[29] Harmonic analyses indicate that the SF Bay admittance ratio $|\mathrm{AD}_{M_2}|$ increased from roughly 1858 to 1987, but has slightly decreased thereafter (Figure 3). Increasing tidal amplitudes are seen at most Northeast Pacific stations, likely due to a combination of large-scale and coastal oceanic processes, and harbor development [*Jay*, 2009; *Woodworth*, 2010]. Because TDE requires estimating flow-induced anomalies in tidal properties, trends in tidal constituents unrelated to river flow could significantly bias flow hindcasts, and long-term alterations in river flow due to multiple and increasing flow diversions over time [*Nichols et al*., 1986] could produce a secular (century scale) increase in tidal constituents. Even though there are no sharp increases in $|\mathrm{AD}_{M_2}|$ associated with the completion of water projects, removal of secular $|\mathrm{AD}_{M_2}|$ trends in a nonbiased way is a key component in hindcasting SF Bay inflow. We assume, to lowest order, that the century-scale trends in tidal properties is unrelated to flow and validate this assumption *ex post facto* by analyses of the 1858–2011 TDE hindcast.

[30] For simplicity, we use a piecewise linear function to remove the trend from the $|\mathrm{AD}_{M_2}|$ time series. To investigate possible bias introduced by trend removal, TDE hindcasts were evaluated for five different physically plausible detrending scenarios and tested against 11 major 20th Century floods. These scenarios are based on alternative hypotheses regarding the causes of the long-term trend. In scenario 1, $|\mathrm{AD}_{M_2}|$ is not detrended, which corresponds to the assumption that all the long-term trend in admittance is

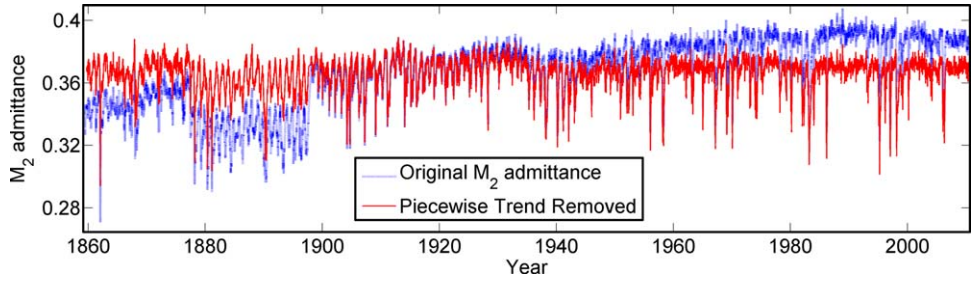

Figure 3. $|\mathrm{AD}_{M_2}|$ with and without detrending.

due to changes in river flow. In scenario 2, a single linear trend over the entire 150 year record is removed, assuming that tidal evolution has been uniform in time and independent of discharge. In scenario 3, high discharge periods are removed from the $|\mathrm{AD}_{M_2}|$ time series, before removing a linear trend from the 150 year record, to reduce any possible bias introduced by an uneven distribution of freshet events and their regulation. In scenarios 4 and 5, variability in tidal evolution (e.g., as might be caused by changing gauge position or historical sedimentation/erosion interacting with changes in coastal tides) is allowed. Thus, a piecewise removal of trends is made using natural breaks in the time series. Four time periods are used: 1858–1877 (Fort Point period), 1877–1897 (Sausalito period), 1897–1987 (Crissy Field period), and 1987–2010 (modern period); the reason for change in trend ca., 1987 is unclear, though the break is obvious. In scenario 4, the full time series is used for detrending, whereas in scenario 5, high-flow periods are excluded, as in scenario 3.

[31] Table 1 lists TDE hindcast flows for each detrending scenario using equation (7), with TPR $= |\mathrm{AD}_{M_2}|$. TDE hidcasts based on $\frac{M_4}{M_2^2}$ are also given for reference (though this method is only realistic for low flows), because $\frac{M_4}{M_2^2}$ shows no trend and does not need to be detrended. Scenario 5, with the lowest root-mean-square (RMS) error between hindcast and measured floods, was used for detrending the $|\mathrm{AD}_{M_2}|$ time series (Figure 3). Although A_{M_4/M_2^2} poorly represents historical floods (Table 1), a scatter plot of A_{M_4/M_2^2} versus river discharge (Figure 4) shows that it exhibits a stronger sensitivity (larger slope) than $|\mathrm{AD}_{M_2}|$ at low flows. We hindcast, therefore, low inflow periods using A_{M_4/M_2^2}, for which detrending is not needed. This lack of trend suggests that the factors affecting overtide generation have not changed greatly over time.

[32] Trend removal interacts, however, with another issue—tides are smaller at Sausalito than at Fort Point, and the mean and variance of $|\mathrm{AD}_{M_2}|$ are systematically smaller during the 1877–1897 period that the gauge was in Sausalito. The admittances were corrected using two degrees of freedom, such that the mean and variance for the 1877–1897 Sausalito $|\mathrm{AD}_{M_2}|$ values were equal to the average of those for 1868–1877 and 1898–1907, when the gauge was at Fort Point.

2.3.4. Regression Analysis and Flow Hindcasts

[33] The parameters α, β, and γ in equation (7) are determined by nonlinear regression analysis of the 1930–1990 NDOI estimates against tidal properties, using the Matlab function (nlinfit). For use in the regression analysis, the weekly T_Tide outputs (and the similarly averaged flows) were bin-averaged in 100 bins, evenly spaced in terms of the tidal property ($|\mathrm{AD}_{M_2}|$ or A_{M_4/M_2^2}). Before bin-averaging, points associated with noisy or incomplete data were removed from the time series of tidal properties. Specifically, we used only M_2 and M_4 amplitudes with a signal-to-noise ratio (SNR) > 10; the SNR statistic is a standard T_Tide output [*Pawlowicz et al.*, 2002].

[34] As shown in Figure 4, the relation between tidal properties and flow is nonlinear, and no single tidal property provided optimal hindcasts through the full range of observed flows. Thus, separate nonlinear regressions were carried out for low (NDOI $< \sim 1000$ m^3 s^{-1}) and high flows (NDOI $> \sim 1000$ m^3 s^{-1}). The ratio A_{M_4/M_2^2} was used for low flows (Figure 4b), with $A_{M_4/M_2^2} < 0.09$, while $|\mathrm{AD}_{M_2}|$ was used for high flows ($|AD_{M_2}| < 0.36$; Figure 4a). This approach to the regression models is justified below in terms of the RMS errors of the 1930–1990 hindcasts, after definition of an error criterion.

[35] A uniform time series of flows was hindcast for 1858–2010 using equation (7), with the regression parameters specified in Table 2. One modification of these hindcast

Table 1. TDE Hindcasts for Different Scenarios Versus Observed Flood Flows in m^3/s

	Year												
Scenario	1938	1942	1956	1958	1970	1983	1986	1995	1997	1998	2006	1862	1881
Observed	5550	6100	5700	5800	7550	8200	6250	7200	6300	6900	5700	–	–
1	6000	6000	6300	5800	5600	6500	5800	6500	5500	5550	4700	14550	9750
2	5350	5700	6500	5750	6350	7800	7300	8400	7400	7500	6900	10800	6850
3	5500	5800	6600	5850	6400	780	7300	8400	7400	7450	6900	11025	7100
4	5450	5700	6550	5800	6350	7800	7300	8350	7200	7200	6000	9500	8600
5	5500	5800	6600	5800	6450	7900	7300	8200	7000	7050	5800	9850	8400
$\frac{M_4}{M_2^2}$Method	4600	4500	4100	4300	3100	4000	3800	4100	3300	3900	3600	5100	4100

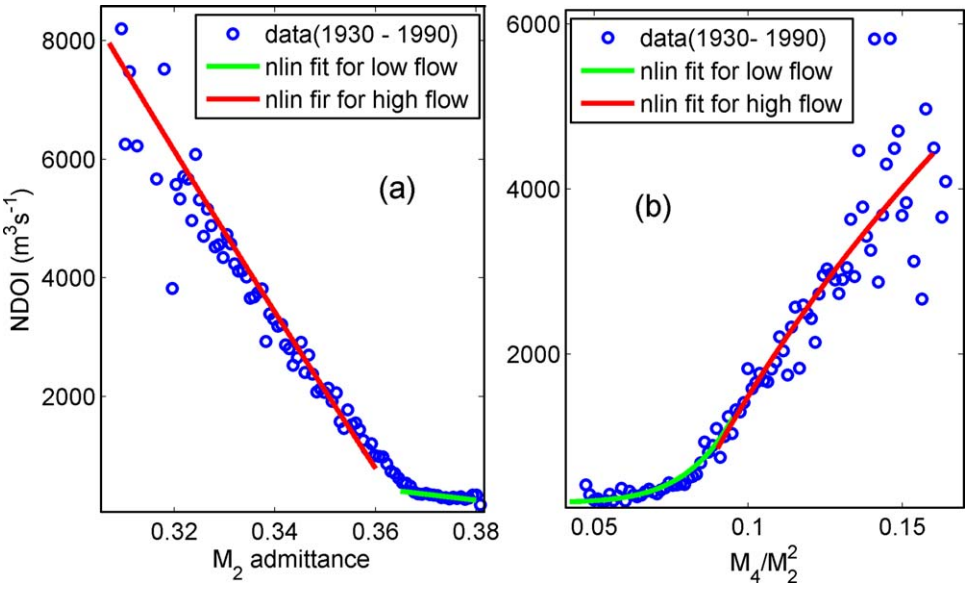

Figure 4. Nonlinear regression: (a) is AD $_{M_2}$, and (b) is $\frac{M_4}{M_2^2}$.

flows was made. During low river flow periods, neap-spring variations in tidal range (neglected in equation (7)) affect flows hindcasts, causing artificial neap-spring variability. A Saviztky-Golay filter was used to remove these fluctuations [*Savitzky and Golay*, 1964]. The Saviztky-Golay filtering method is better than a moving average filter because it tends to preserve data features such as peak height and width, which are usually attenuated by the moving average filter [*Guinon et al*., 2007].

2.3.5. Error Propagation

[36] There are uncertainties associated with river flow hindcasts that must be quantified by statistical methods. A Monte Carlo analysis is used here to define the 95% confidence intervals of the estimates. In a Monte Carlo simulation, the behavior of a statistic in random samples is assessed by the empirical process of drawing many random samples and observing their behavior [*Mooney*, 1997]. For estimating confidence intervals by Monte Carlo analysis, it is necessary to determine the standard deviation (σ) of each parameter, determined by T-Tide for each component for each analysis window [*Pawlowicz et al*., 2002], and then propagate the individual parameter errors to determine errors in regression variables. For the standard deviation of $|\mathrm{AD}_{M_2}|$ ($\sigma_{AD_{M_2}}$), we have

$$\sigma_{AD_{M_2}} = \frac{\sqrt{\sigma_{A_{M_2}}^2 + A_{M_2}^2 \sigma_{\theta_{M_2}}^2}}{\hat{A}} \tag{11}$$

Table 2. Estimated Coefficients in Equation (7)

	$\lvert\mathrm{AD}_{M_2}\rvert$		$A_{\frac{M_4}{M_2^2}}$	
	Low Flows	High Flows	Low Flows	High Flows
α	4.8398 E+05	1.0555 E+05	205.8077	−4.2415 E+04
β	−4.8758 E+05	−1.6505 E+05	1.8903 E+09	6.0315 E+04
γ	0.0083	0.4454	6.1302	0.1379

where $\sigma_{A_{M_2}}$ is the standard deviation of A_{M_2} and $\sigma_{\theta_{M_2}}$ is the standard deviation of θ_{M_2}. The standard deviation of $M_4/M_2^2$is

$$\sigma_{A_{\frac{M_4}{M_2^2}}} = A_{\frac{M_4}{M_2^2}} \times \sqrt{\left(\frac{\sigma_{A_{M_4}}}{A_{M_4}}\right)^2 + 2 \times \left(\frac{\sigma_{A_{M_2}}}{A_{M_2}}\right)^2}. \tag{12}$$

[37] For comparison to the uncertainties derived for our TDE estimates below, we note that any river instrumental discharge measurement can be assumed to have a 95% confidence limit of ±5% [*Di Baldassarre and Montanari*, 2009].

[38] Monte Carlo simulations were carried out based on 5000 ensembles. Using nonlinear regression, α, β, and γ in equation (7) were calculated for each ensemble. As Figure 5a shows, the distribution of coefficients is approximately Gaussian, and the 95% confidence interval limits can be estimated from the 2.5 and 97.5% quantiles. While somewhat more than 95% of the observed data fall within the 95% confidence interval, errors are dependent on flow and the method is more reliable for high flows than during dry periods (Figure 5b).

2.3.6. Model Selection

[39] As described above, $|\mathrm{AD}_{M_2}|$ and A_{M_4/M_2^2} models were used for NDOI > 1000 m^3 s^{-1} and NDOI < 1000 m^3 s^{-1}, respectively. This choice can be justified *ex post facto* in terms of RMS errors for the 1930–1990 calibration period (Figure 6). For SF Bay at least, use of statistics related to quadratic overtide M_4 appears to provide the best hindcasts during low river flow periods. RMS errors for low-flow events estimated using the $|\mathrm{AD}_{M_2}|$ model are ∼1000 m^3 s^{-1}, larger than the flows. In contrast, the RMS errors for the A_{M_4/M_2^2} model are ≤ 500 m^3 s^{-1}.

3. Results and Discussion

3.1. Validation of the TDE Model

[40] Hindcast flows were validated using four series of data: (a) NDOI for 1930–2010 (Figure 7), (b) the daily

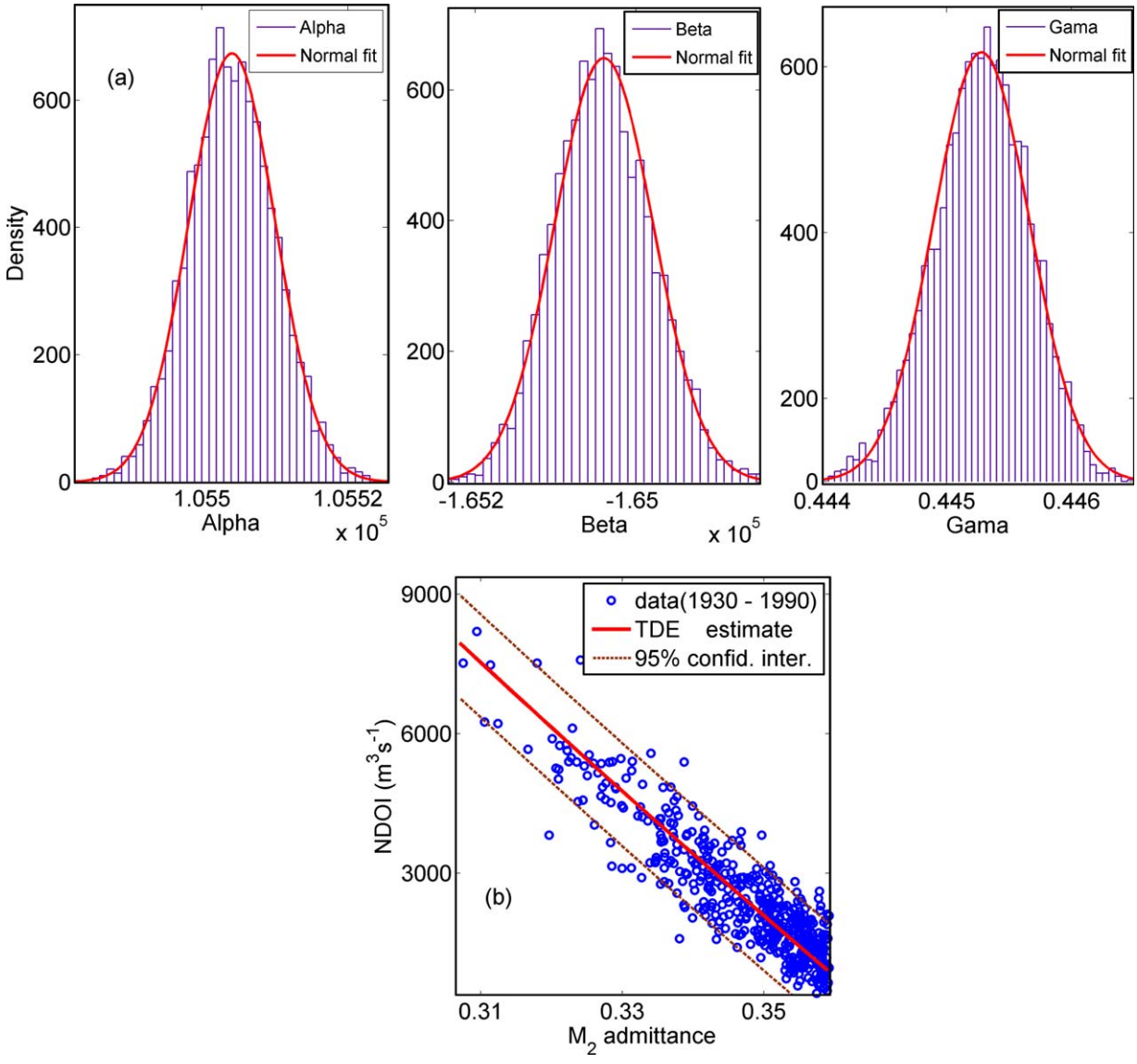

Figure 5. (a) Distribution of coefficients α, β, and γ in equation (7) for high river flow estimation using $|\mathrm{AD}_{M_2}|$ and (b) estimated NDOI for high-flow periods and 95% confidence interval limits versus $|AD_{M_2}|$ based on Monte Carlo analysis.

flow at Red Bluff (1891–1944; Figure 8), (c) the monthly averaged eight-river flow index (1906–2010; Figure 9), and (d) monthly precipitation data at SF (1850–2010; Figure 10).

3.1.1. Comparison to NDOI

[41] The efficacy of the hindcasts for the calibration period (1930–1990) can be seen in Figures 7a and 7b, and Table 3. The TDE time series for 1980–1984 (Figure 7b) shows that the major flood of 1983, the moderate freshets in 1980, 1982, and 1984, and the low-flow period of 1981 are all reproduced by the hindcast. Some details of the hindcast flow differ from the measured flow and account for some of the scatter in Figure 7a; in particular, the hindcast discharge sometimes lags the measured NDOI by several days (see section 3.2 for discussion).

[42] Another way to test the model is to compare hindcasts with observations for a validation period not used for calibration. The result shows good agreement between TDE estimated flows and calculated NDOI (Nash-Sutcliffe coefficient equal to 0.902; Table 3). In addition, 1991–2010 NDOI is compared with the TDE hindcast (Figure 7c). TDE hindcasts generally exhibit errors $\leq$20%; the RMS error is 343 $m^3 s^{-1}$. They are especially successful during high river flows (errors usually $\leq$10%, RMS error $=$551 $m^3\ s^{-1}$), when the alteration of tidal properties is large. Figure 7d shows TDE modeled flows with estimated 95% confidence intervals from 1996 to 2000. As in Figure 7b, the overall pattern and major peaks are captured, but the hindcast and observed flows in Figures 7b and 7d do not always rise or fall at the same rate. TDE hindcasts also underestimate some peaks, but the differences fall within the estimated 95% confidence interval for most high-flow periods and most periods of nearly steady flow. One possible reason for differences in timing and magnitude of peaks between observations and TDE hindcasts is that tidal properties are likely affected to some degree by salinity

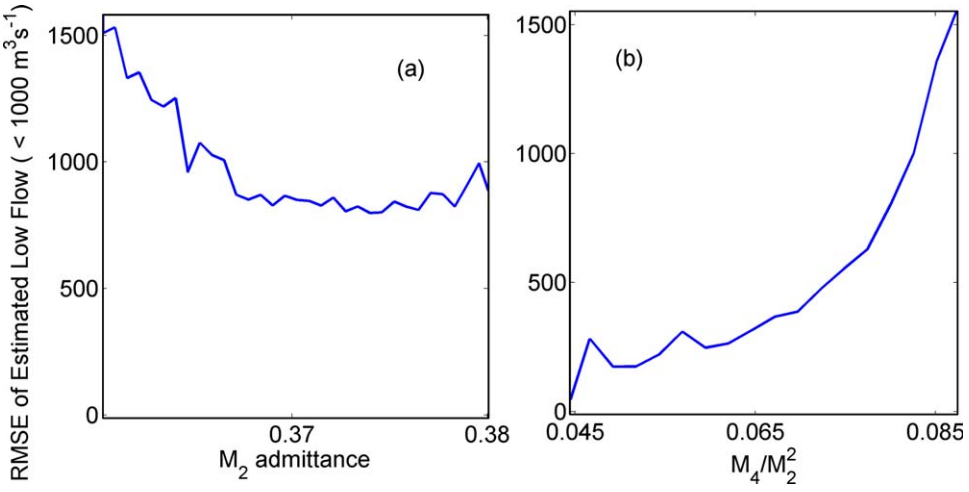

Figure 6. Root mean square error (RMSE) during low flow periods for: (a) $\mathrm{AD}_{M_2} > 0.36$ and (b)$A_{\frac{M_4}{M_2^2}} < 0.09$.

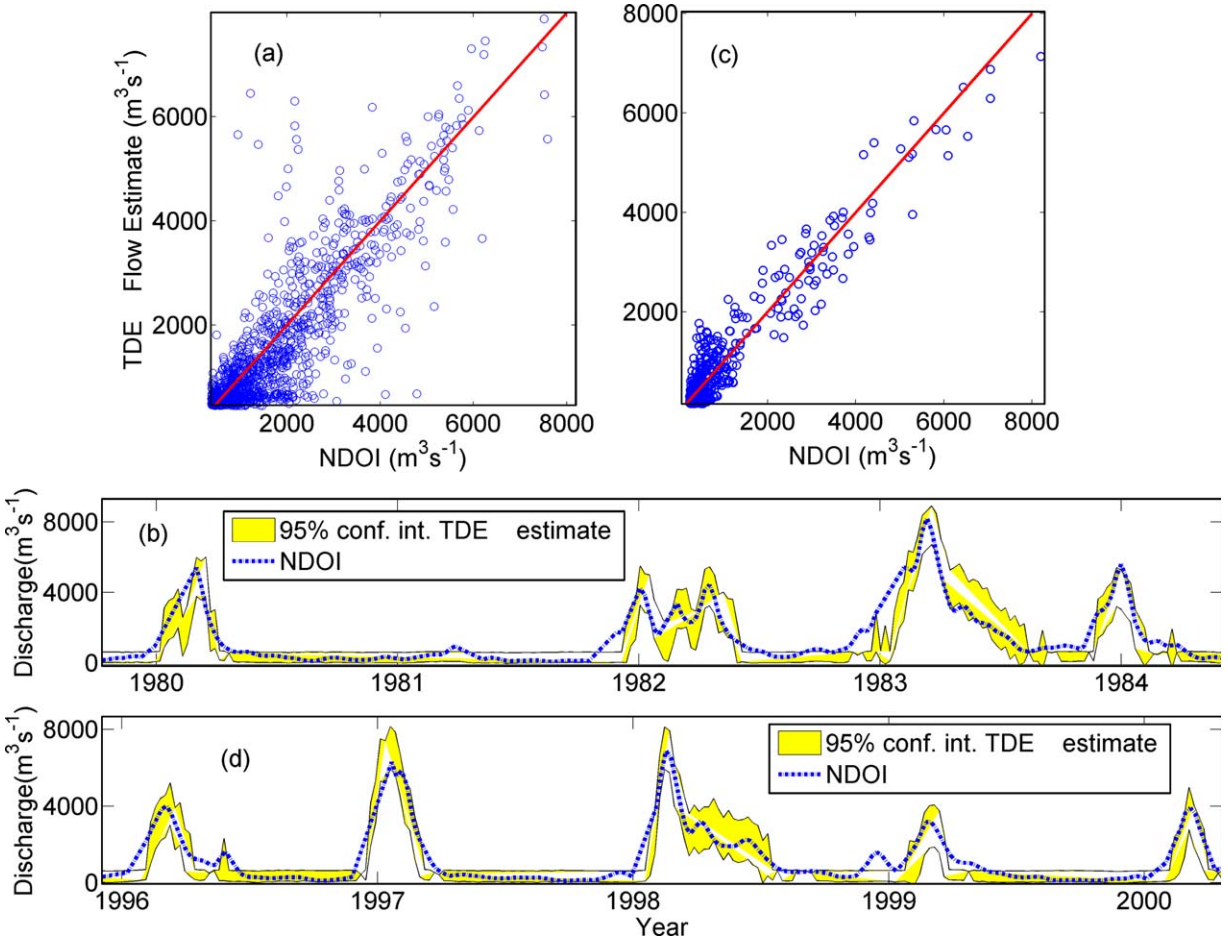

Figure 7. Comparison of estimated flows with observations: (a) scatterplot of TDE hindcast versus NDOI flows for the calibration period 1930–1990, (b) time series of hindcast TDE flows (with 95% confidence limits) and NDOI for 1980–1984, (c) scatterplot of TDE hindcast versus NDOI for 1991–2010, and (d) time series of hindcast TDE flows (with 95% confidence intervals) and NDOI for 1996–2000.

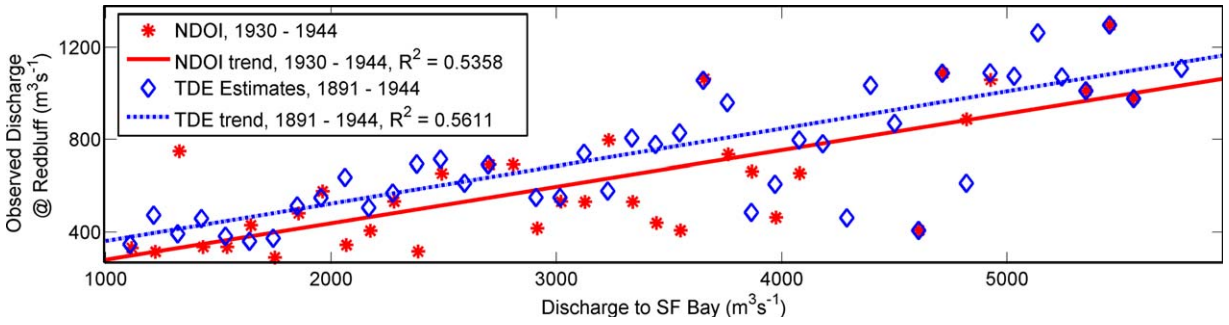

Figure 8. Maximum yearly pseudo-NDOI (red stars and red line) and TDE hindcast flows (blue diamonds and blue dash-line) versus observed maximum annual Red Bluff flows.

intrusion, and the adjustment time for the salt distribution in SF Bay due to changes in river flow is several weeks [*Monismith et al*., 2002].

3.1.2. Comparison to Flow at Red Bluff

[43] Measured flows at Red Bluff (USGS 11377100), available daily from 1891 to present, can also be used to assess TDE hindcasts. While this gage measures the flow from only 14% of the basin, it provides a valuable check before 1930, when NDOI is not available. To compare Red Bluff flows with our hindcast, we plot observed Red Bluff flows against bin-averaged NDOI over the period 1930–1944 (i.e., using data from before the Shasta Dam came online; Figure 9). Red Bluff flows are similarly plotted against bin-averaged TDE hindcast flows for 1891–1944 (Figure 8); regression lines were fitted in both cases. The slopes of the two flow estimates (0.156 ± 0.025 and 0.171 ± 0.016) agree within their mutual 95% confidence limits, the adjusted R^2 are very similar (0.536 for the NDOI line versus 0.561 for the TDE line), and there is a zero offset of 125–176 $m^3\ s^{-1}$ (again similar within 95% confidence limits, ± 59 and ± 82 $m^3\ s^{-1}$, respectively). These results suggest that there is no systematic error within the TDE before 1930, and random errors may cause the slight difference in slope, offset, and R^2 values [*Taylor*, 1997].

3.1.3. Comparison to the Eight-River Flow Index

[44] Another way to assess the robustness of TDE is to compare our hindcast flows to measures of unimpaired SF Bay inflow. Figure 9 shows the yearly averaged TDE flow estimates versus the Eight-River Index or ERI (both averaged over December–May) for the periods 1906–1929 and 1930–2010. The TDE and ERI measures are well correlated in both time periods (R^2 is 0.848 and 0.813 before and after 1930, respectively), but the slope of the fitted line is different before (0.0917) and after (0.0565) 1930. Several flow management factors may contribute to this decrease in slope, including diversion and reservoir storage beyond May.

3.1.4. Comparison With Precipitation Data

[45] Precipitation data can also be used to check the accuracy of TDE hindcasts. Figure 10 shows annual San Francisco precipitation and TDE modeled annual average flows, 1858–2010. In general, the precipitation record agrees with the estimated river flow, with large rainfall years producing correspondingly large annual flows. Precipitation data also strongly support the peak TDE flow measured in January 1862 (Figure 11), as the 2 month rainfall total of 861 mm measured from December 1861 to January 1862 is 25% greater than the next largest total (685 mm in January–February 1998). The San Francisco precipitation data are consistent with monthly data for Sacramento for 1852–1862 [*Logan*, 1864], which indicate that 219, 382, and 108 mm of rainfall fell in the 3 months from December 1861 to February 1862, respectively. Moreover, the rain-on-snow events of December 1861 and January 1862 removed the snowpack in the Sierra mountains [e.g., *Hunsaker and Curran*, 2005], significantly increasing the flood intensity.

[46] Interestingly, the TDE hindcast suggests that the annual flow from the 1861–1862 winter was smaller than the next two largest rainfall years in 1889–1890 and 1997–1998. Examination of the precipitation data shows that rainfall in 1861–1862 was concentrated over a shorter period than in 1889–1890 and 1997–1998, and led to a larger flood but, apparently, a smaller annual flow. The different annual flows also could be caused by differences in evapotranspiration, storage, diversion, and infiltration between

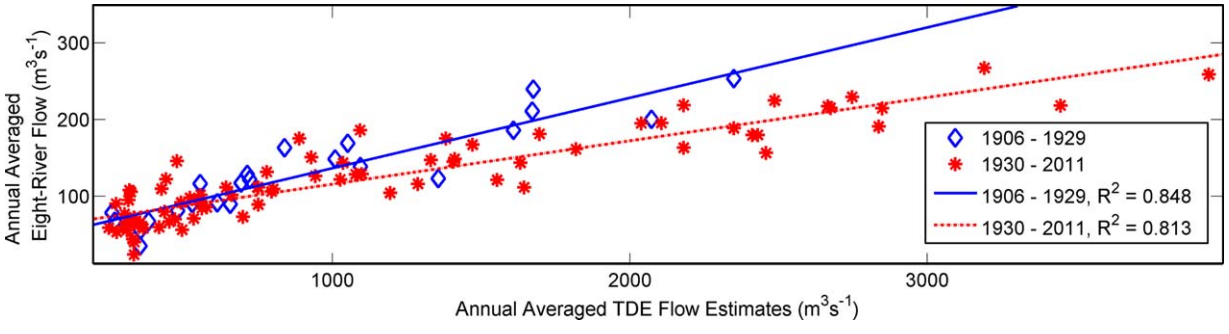

Figure 9. Annual averaged TDE flow estimates versus annual averaged Eight-River flow index.

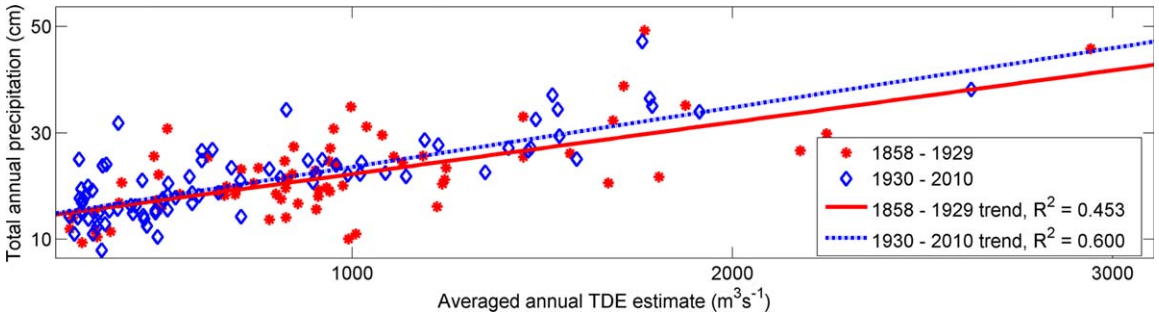

Figure 10. Annual precipitation at San Francisco versus hindcast annual average TDE for 1858–2010.

the water years [see e.g., *Hamlet and Lettenmaier*, 2007]. Indeed, the spring-freshet in 1862 was small, while the relatively large spring freshet in 1890 shows that there was significant snowpack storage (Figure 11). It is also possible that missing data in May–June 1862 caused an underestimate of the 1862 freshet [see *Talke and Jay*, 2013]. Finally, because rainfall is spatially variable, the local rainfall data in Figure 10 are only an approximate indication for precipitation over the watershed. Nonetheless, the qualitative agreement between precipitation and estimated flow in Figure 10 support the validity of TDE.

3.2. TDE Hindcasts

3.2.1. Magnitude of the Great 1862 Flood

[47] The above results suggest that TDE successfully captures trends and magnitude of observed river flow, 1930–2010. Tidal data for 1858–1929 allow us to provide novel discharge hindcasts for the years prior to 1930, for which NDOI estimates are not available. A plot of the TDE hindcast for 1858–2010 shows that the 1862 flood is the largest flow event of the last 150 years (Figure 11). Specifically, the TDE hindcast for January 1862 shows a peak 18 day flow of 9850 m^3s^{-1}, 25 ± 20% larger than the peak flood in January 1997 (similarly averaged), which is the largest flow in the NDOI record. Precipitation data 1858–2010 (Figure 10) supports this conclusion—winter 1862 is the wettest season in the entire precipitation record. *Hunsaker and Curran* [2005], modifying a method developed by the Corps of Engineers, argued that the instantaneous peak flow for the 1862 was the largest in the last 150 years and 32% greater than in 1997; this estimate is based, however, on only ∼8% of the total Sacramento River basin area. While monthly SF precipitation similar to that in January 1862 occurred in 1853, 1867, 1881, 1986, and 1997, the heavy rains of January 1862 were preceded by very high precipitation in December 1861. The duration of heavy rainfall, the antecedent snowpack, and the rapid snowmelt together make the flooding in January 1862 the dominant flood event of the last 150 years. Accordingly, this series of storms served as the historic basis for the USGS ARkStorm study (http://wdr.water.usgs.gov/), a recent attempt to estimate the consequences of a truly catastrophic, California-wide flood.

Table 3. Model Efficiency Coefficients

Time Span	Nash-Sutcliffe Coefficient
1930–1990	0.727
1991–2010	0.902

3.2.2. Changes in the Annual Hydrograph

[48] The TDE hindcasts also allow evaluation of long-term changes in the annual hydrograph. Figure 12a compares 40 year TDE hindcasts averaged by year-day for the late 19th century (1858–1898) and modern era (1968–2008). Both the timing and magnitude of the annual peak flow has changed considerably over time, which is consistent with the results of other studies [*Ganju et al*., 2008; *Aguado et al*., 1992]. Before 1900, the snowmelt-driven peak flow of ∼1850 m^3s^{-1} typically occurred in early May. The contemporary peak (∼1700 m^3s^{-1}) is ∼10% smaller and normally occurs between January and March, roughly coincident with peak precipitation. Historic summer flows were 100–300 m^3s^{-1} larger than at present, and the minimum flow of 400 m^3s^{-1} occurred on average in November. The present minimum flow of ∼300 m^3s^{-1} occurs about 1 month earlier. Dominant reasons for these changes are as follows:

3.2.2.1. Flow Control and Diversion

[49] In the 19th century, before construction of storage reservoirs, most peak flows occurred due to a spring snowmelt. During the 20th century, flood control and diversion for irrigation and human consumption reduced total flows and contributed to the movement of peak flows to winter or early spring [*Nichols et al*., 1986; *Knowles*, 2002].

3.2.2.2. Climate Change

[50] Change in the amount and timing of precipitation and the seasonal temperature cycle may also have affected the magnitude and timing of runoff, though temperature increases have greatly outweighed changes in precipitation. A dominant fraction of river flow in the watershed originates from melting snowpacks, and increasing temperature results in increased winter runoff and earlier peak spring river flows [*Hamlet et al*., 2005; *Cayan et al*., 2001; *Hamlet and Lettenmaier*, 2007]. Climate scenarios suggest further decreases in precipitation and earlier snowmelt [*Hamlet et al*., 2005; *Leung et al*., 2004].

[51] TDE hindcasts suggest that the above changes have resulted in a ∼30% decrease in annual average discharge after 1900 (∼2.1 km^3), compared to the 19th century (∼ 2.7 km^3), a decrease of ∼29%. *Nichols et al*. [1986] suggests that modern inflow to the bay is ∼40% below historic levels ca. 1850. Given uncertainties in both estimates, they are in approximate agreement.

[52] The timing of high-flow periods and flood has also changed. This is demonstrated for 1858–1898 and 1968–2008 by plotting against year day the 97.5% exceedance

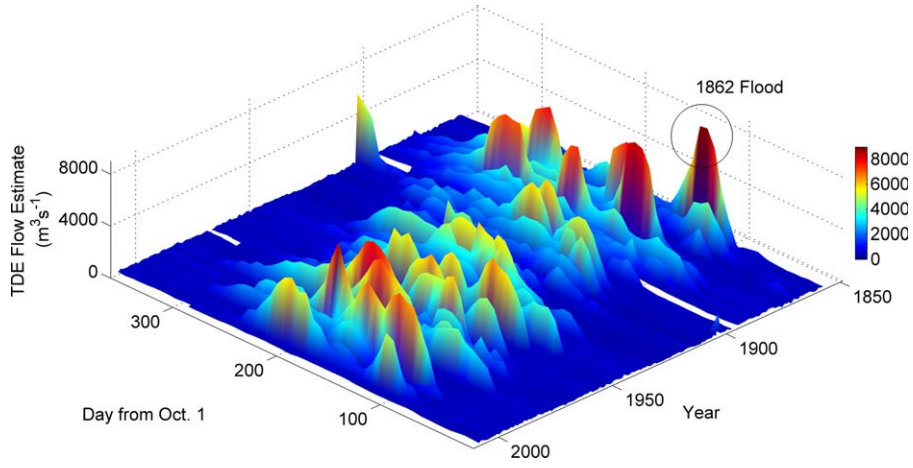

Figure 11. TDE hindcasts of annual hydrographs, 1858–2010.

values (the flow exceeded only 2.5% of the time for any given year day) (Figure 12b). Before 1900, high-flow events occurred primarily in winter (January and February) and late spring (May and June). During the 20th century, large flows have most often occurred in March and April. The hindcast flows for 1858–2010 also support this conclusion (Figure 11) and emphasize that spring freshets, common in the late 19th century, were much less frequent after 1900 (even before significant flow regulation) and essentially vanished after Shasta Dam was completed in 1944. The large event in autumn 1904 (evident in Figure 11) is unique in the record, which suggests that it might be an anomaly due to faulty tide data. In fact, gauge comparisons from 1904 indicate that some clogging occurred due to sedimentation on 7 September (probably from a storm), and resulted in water level errors of 0.1–0.3 m over the next month [see also *Talke and Jay*, 2013]. Hence, the reduced admittance may be in part due to gauge issues. However, precipitation records indicate that 129 mm of precipitation fell in September 1904 in San Francisco, more than in any other September between 1849 and 2011 (http://ggweather.com/sf/ monthly.html). Thus, the event appears to be real, though perhaps the peak flow has been overestimated. The fact that the event cannot be traced in any of the USGS fluvial flow/elevation records available for this time period emphasizes the importance of estimating flows closer to the ocean. Finally, while there are a few early winter (December) events before 1900, these become much more prominent after about 1940; this may be due in part to flow regulation after 1944; i.e., emptying of reservoirs in early winter during wet years.

[53] Monthly averaged TDE hindcasts are listed by water year, from 1859 to 2010, in Table S1 in supporting information.

3.3. Error Analysis

[54] Evaluating the significance of the TDE hindcast flows requires understanding the magnitude of likely errors, which may be systematic (due to bias) or random. Random errors associated with estimates are reflected in the confidence intervals (e.g., Figure 7), but systematic errors are not. We consider here the likely importance of both kinds of errors.

3.3.1. Systematic Errors

[55] TDE estimates are sensitive to the method used to detrend tidal admittances, and this is the most likely source of systematic error. As discussed in section 2.3.3, there has been a secular (century scale) increase in $|AD_{M_2}|$ at SF that

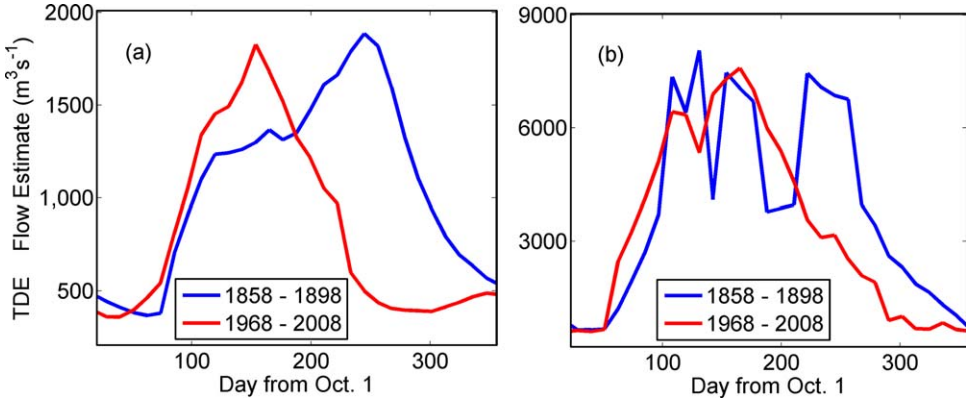

Figure 12. (a) TDE hindcasts of flow by year day, averaged over 40 years for 1858–1898 and 1968–2008 and (b) 97.5% flow exceedance by year day, for the same periods.

reflects in part changes in ocean tides, but may also reflect changes SF Bay bathymetry and shorelines. This must be removed to avoid aliasing of discharge estimates. We have used the simplest reasonable approach to de-trending, piecewise linear removal, which adequately accounts for the exogenous factors (e.g., bathymetric changes). Comparing different possible scenarios (Table 1), we chose a scenario that minimized errors associated with TDE hindcasts of selected 20th Century flood events. As shown in Table 1, choosing a different detrending approach can considerably alter the estimates for some 19th Century floods. For example, the five detrending scenarios described in Table 1 lead to a peak flow in January 1862 that ranges from 9500 to 14,550 $m^3\ s^{-1}$ (Table 1). Our adopted TDE hindcast 18d average flow, 9850 $m^3\ s^{-1}$, is near the low end of the estimate. The wide range of possible flows for this event reflects both its real magnitude and its position near the beginning of the time series, which produces a large difference between scenario 1 (no trend removal) and other scenarios. On the other hand, our adopted estimate for the 1881 flood, 8400 $m^3\ s^{-1}$, is above the average for the five scenarios, and the range for this event is smaller (6850–9750 $m^3\ s^{-1}$; Table 1) than for the 1862 flood. Clearly, the choice of the detrending scenario affects the TDE hindcast flows before 1900. In general, if detrending had not been used (which we regard as quite unrealistic, given that tidal amplitudes are increasing throughout the northeast Pacific [*Jay*, 2009]), predicted flows would have been much higher for this time period.

[56] The treatment of the 1877–1897 period when the tide gauge was in Sausalito is also important, because the M_2 tide was systematically smaller by ~10% at this location, relative to Fort Point. We have used the simplest reasonable correction, adjustment of the mean and standard deviation of $|AD_{M_2}|$ for this time period.

[57] Imperfect conceptual modeling of the tidal-fluvial interactions by equation (7) is also a possible problem. TDE is based on an approximate inversion of a tidal wavenumber model for a single, incident tidal wave. Given that the SF tide gauge is located at the estuary mouth, the incident wave is unlikely, at that location, to reflect the state of the friction in the estuary. It is likely that the gauge is responding to modification of both the incident and reflected wave; fortunately, the wavenumbers for both waves scale with discharge in the same manner. Tidal properties may also respond to other factors correlated with river flow. A change in salinity intrusion length may change the friction on a tidal wave [*Giese and Jay*, 1989]. Thus, the tidal admittance variations used here to gauge discharge may in part be a response to changes in salinity intrusion length driven by river discharge. While this is an issue of theoretical interest, it is of little practical importance. Finally, high flows in SF Bay from winter storms are correlated with high water levels [*Bromirski and Flick*, 2008]. Elevated water levels may also affect tides by changing friction and/or residence time. This does not appear to be a major issue—high flows are more accurately modeled than low flows—but it may contribute to scatter in the results.

[58] Systematic errors in the 1930–1990 NDOI estimates used for TDE calibration must also be considered, particularly before 1956, when fewer data were available for DAYFLOW calculations, and these might distort TDE hindcasts. DAYFLOW routing is particularly difficult during low flows when tidal current reversals extend far up into delta channels. Indeed, the lowest flows during the calibration period occurred before 1956, and TDE hindcast errors are largest and most variables for low flows. Still, the errors in low-flow TDE hindcasts during the calibration period are not strongly biased. Thus, systematic errors seem unlikely or would affect all TDE hindcasts uniformly and have, therefore, little impact on historic comparisons.

3.3.2. Random Errors

[59] Random errors associated with tidal measurements can arise from various difficulties with the gauge and data reduction. Our examination of a selection of the original marigrams from which the hourly tidal data were compiled does not suggest any systematic errors, and random errors ("data noise") are quantified in the T_Tide estimates and were used to determine overall TDE uncertainties as per equations (11) and (12). The completeness of the tidal data and overall high quality of the record minimize this source of error. Net inflow to the Bay cannot be measured directly and is routed (as NDOI) using the data gathered at upstream stations. Random errors related to infiltration and evaporation estimates likely contribute to the divergence of TDE and NDOI estimates, as may errors in the assumed lags used in compiling NDOI. The latter may contribute to differences in both the timing and absolute values of peak flows, as well as the shape of the hydrograph associated with high-flow events. Nonstationarity in river flow over the period of harmonic analysis may also contribute to TDE errors.

3.4. Future Improvements

[60] NDOI includes the 90% of the total freshwater discharge to SF Bay that comes from the Sacramento River delta, as noted above. Because we have calibrated our TDE estimates to NDOI, our present calculation also includes only the input to SF Bay from the delta, not the total flow to the ocean. While the estimates presented here could be scaled up by a uniform 10% to account for local creeks and rivers, local inflow is likely distributed differently in time than delta inflow. Thus, a more sophisticated procedure, perhaps based on correlation of local precipitation data with local stream flow records should be used, an effort we will not attempt here [but see *Ganju et al*., 2008].

[61] Our TDE estimates are also imperfect because they average over tidal monthly variations in delta storage, due to the 761 h tidal analysis window. A future analysis based on short, continuous wavelet transform windows (in the manner of *Jay and Kukulka* [2003]) would provide flow estimates with a higher inherent time resolution. Moreover, TDE could be improved by using two stations. In a two-station analysis, the amplitude admittance ratio is formed using the fluctuations in tidal constituents at a more landward station. The more seaward gauge is then used to eliminate fluctuations in ocean conditions in equation (3a)–(3c), rather than the astronomic tidal potential V. Finally, it would be useful to determine whether tidal properties could be used as a proxy for historic salinity intrusion, presently quantified by the X2 metric (the distance to the salinity =2 isopycnal; www. water.ca.gov/dayflow/).

[62] Recent studies suggest that, within a deltaic channel network, flow division at tidal junctions is affected by

neap-spring variations in tidal range [*Buschman et al.*, 2010; *Sassi et al.*, 2011b]. Use of TDE to examine this division between distributaries would be an interesting and important challenge.

3.5. Broad Utility

[63] The actual value of any indirect flow estimation method like TDE can only be determined by experience—Can its success in SF Bay be replicated elsewhere? Preliminary results suggest that it can also be used in the Columbia [*Jay and Kukulka*, 2003] and Fraser Rivers. The choice of hindcast parameters and other details are, however, system specific. Also, it may be advantageous to substitute a coastal (or near-coastal) tide gauge for the astronomical potential, if a second gauge is available. A second gauge is unlikely to be available, however, for hindcasting, as here, historical flows. To the degree that tide gauges are located seaward of typical river gauges and often have longer records, the method presented here should be applicable on a global basis.

4. Summary and Conclusions

[64] The discharge of large tidal rivers to the ocean is an important issue for the global water balance, sediment input to the ocean, climate analyses and characterization of natural variability, and water resources management. However, this discharge is often difficult to determine, as illustrated by the case of San Francisco (SF) Bay. Uncertainty in the timing and magnitude of freshwater inflow to SF Bay exists because the delta through which most freshwater reaches the bay is a network of channels with numerous connections, inputs and outputs. Because of these issues, the presently used NDOI is an imperfect measure. In this study, tidal constituents, astronomical forcing and a model of the frictional interaction of flow and tides were used to hindcast monthly averaged river flows into SF Bay via a tidal discharge estimation method (TDE). Results show that the M_2 admittance provides the best TDE estimates during periods of high river flow. In dry periods, tidal wave distortion becomes more dominant and higher harmonics are best used for the TDE hindcast. The TDE model was calibrated with 1931–1990 NDOI data, and validated using: (a) NDOI for 1991–2011; (b) the gauged discharge 1891–1944 at Red Bluff, CA; (c) the Eight River Index (1906–2011); and (d) the 1858–2010 SF precipitation record. The annual hydrograph of inflow to SF Bay has changed considerably over time, due to both human alteration and climate change. Before 1900 peak flows were in spring (May and June) but now they occur in winter. However, our hindcast indicates that the largest flood on record occurred in January 1862 (as measured by an 18 day average) and was about 25% larger than the 1997 flood.

[65] **Acknowledgments.** Support for this project was provided in part by a Miller Foundation grant to the Institute of Sustainability and Systems at Portland State University and a Portland State Research enhancement grant. D.A. Jay and S.A. Talke were supported in part by the National Science Foundation grant: Secular Changes in Pacific Tides, OCE-0929055. S.A. Talke was supported in part by National Science Foundation grant: 19th Century US West Coast Sea Level and Tidal Pproperties, OCE-1155610. Support for P.D. Bromirski from the California Department of Boating and Waterways Oceanography Program is greatly appreciated. We thank David Schoellhamer of the US Geological Survey for his very helpful comments.

References

Aguado, E., D. Cayan, L. Riddle, and M. Roos (1992), Climatic fluctuations and the timing of West Coast streamflow, *J. Clim.*, *5*, 1468–1483.

Bromirski, P. D., and R. E. Flick (2008), Storm surge in the San Francisco Bay/Delta and nearby coastal locations, *Shore Beach*, *76*, 29–37.

Bromirski, P. D., R. E. Flick, and D. R. Cayan (2003), Storminess variability along the California coast: 1858–2000, *J. Clim.*, *16*, 982–993.

Buschman, F. A., A. J. F. Hoitink, M. van der Vegt, and P. Hoekstra (2009), Subtidal water level variation controlled by river flow and tides, *Water Resour. Res.*, *45*, W10420, doi:10.1029/2009WR008167.

Buschman, F. A., A. J. F. Hoitink, M. van der Vegt, and P. Hoekstra (2010), Subtidal flow division at a shallow tidal junction, *Water Resour. Res.*, *46*, W12515, doi:10.1029/2010WR009266.

Cartwright, D., and A. C. Eden (1973), Corrected table of tidal harmonics, *Geophys. J. R. Astron. Soc.*, *33*, 253–264.

Cayan, D. R., S. A. Kammerdiener, M. D. Dettinger, J. M. Caprio, and D. H. Peterson (2001), Change in the onset of spring in the western United States, *Bull. Am. Meteorol. Soc.*, *82*, 399–415.

Cheng, R. T., and J. F. Gartner (1985), Harmonic analysis of tides and tidal currents in south San Francisco Bay, California, *Estuarine Coastal Shelf Sci.*, *21*, 57–74.

Chua, V. P., and O. B. Fringer (2011), Sensitivity analysis of three-dimensional salinity simulations in North San Francisco Bay using the unstructured-grid SUNTANS model, *Ocean Modell.*, *39*, 332–350.

Cloern, J. E., A. E. Alpine, B. E. Cole, R. L. J. Wong, J. F. Arthur, and M. D. Ball (1983), River discharge controls phytoplankton dynamics in the northern San Francisco Bay estuary, *Estuarine Coastal Shelf Sci.*, *16*, 415–429.

Cloern J. E., T. M. Powell, and L. M. Huzzy (1989), Spatial and temporal variability in south San Francisco Bay (USA). II. Temporal change in salinity, suspended sediments, and phytoplankton biomass and productivity over tidal time scales, *Estuarine Coastal Shelf Sci.*, *28*, 599–613, doi:10.1016/0272–7714(89)90010-3.

Conomos, T. J., and D. H. Peterson (1977), Suspended-particle transport and circulation in San Francisco Bay, An overview, in *Estuarine Processes*, vol. *2*, pp. 82–97, Academic, New York.

Di Baldassarre, G., and A. Montanari (2009), Uncertainty in river discharge observations: A quantitavtive analysis, *Hydrol. Earth Syst. Sci.*, *13*, 913–921.

Doodson, A. T. (1957), The analysis and prediction of tides in shallow water, *Int. Hydrogr. Rev.*, *33*, 85–126.

Dronkers, J. J. (1964), *Tidal Computations in Rivers and Coastal Waters*, pp. 296–304, North-Holland, New York.

Flick, R. E., and L. C. Ewing (2009), Sand volume needs of southern California beaches as a function of future sea-level rise rates, *Shore Beach*, *77*(4), 36–45.

Gan, J., L. Li, D. Wang, and X. Guo (2009), Interaction of a river plume with coastal upwelling in the northeastern south China Sea, *Cont. Shelf Res.*, *29*, 728–740.

Ganju, N. K., N. Knowles, and D. H. Schoellhamer (2008), Temporal downscaling of decadal sediment load estimates to daily interval for use in hindcast simulations, *J. Hydrol.*, *394*, 512–523.

Giese, B. S., and D. A. Jay (1989), Modeling tidal energetics of the Columbia River Estuary, *Estuarine Coastal Shelf Sci.*, *29*, 549–571.

Gilbert, G. K. (1917), Hydraulic-mining debris in the Sierra Nevada, *U.S. Geol. Surv. Prof. Pap.*, *105*, 148.

Godin, G. (1985), Modification of river tides by the discharge, *J. Waterw. Port Coastal Ocean Eng.*, *111*(2), 257–274.

Godin, G. (1999), The propagation of tides up rivers with special considerations on the upper Saint Lawrence River, *Estuarine Coastal Shelf Sci.*, *48*, 307–324.

Guinon, J. L., E. Ortega, J. Garcia-Anton, and V. Perez-Herranz (2007), Moving average and Savitzki-Golay smoothing filters using Mathcad, paper presented at International Conference on Engineering Education—ICEE 2007, International Network on Engineering Education and Research (iNEER), Coimbra, Portugal, Sep.

Hamlet, A. F., and D. P. Lettenmaier (2007), Effects of 20th century warming and climate variability on flood risk in the western U.S., *Water Resour. Res.*, *43*, W06427, doi:10.1029/2006WR005099.

Hamlet, A. F., P. W. Mote, M. P. Clark, and D. P. Lettenmaier (2005), Effects of temperature and precipitation variability on snowpack trends in the western United States, *J. Clim.*, *18*, 4545–4561.

Hoitink, A. J. F., F. A. Buschman, and B. Vermeulen (2009), Continuous measurements of discharge from a horizontal ADCP in a tidal river, *Water Resour. Res.*, *45*, W11406, doi:10.1029/2009WR007791.

Hunsaker, L., and C. Curran (2005), *Lake Sacramento—Can it Happen Again?*, pp. 105, Acad. Print., Grants Pass, Oregon.

Inman, D. L., and S. A. Jenkins (1999), Climate of small California rivers, *J. Geol.*, *107*, 251–270.

Jay, D. A. (1991), Green's law revisited: Tidal long wave propagation in channels with strong topography, *J. Geophys. Res.*, *96*, 20,585–20,598.

Jay, D. A. (2009), Evolution of tidal amplitudes in the eastern Pacific Ocean, *Geophys. Res. Lett.*, *36*, L04603, doi:10.1029/2008GL036185.

Jay, D. A., and E. P. Flinchem (1997), Interaction of fluctuating river flow with a barotropic tide: A test of wavelet tidal analysis methods, *J. Geophys. Res.*, *102*, 5705–5720.

Jay, D. A., and E. P. Flinchem (1999), A comparison of methods for analysis of tidal records containing multi-scale non-tidal background energy, *Cont. Shelf Res.*, *19*, 1695–1732.

Jay, D. A., and T. Kukulka (2003), Revising the paradigm of tidal analysis—The uses of non-stationary data, *Ocean Dyn.*, *53*, 110–123.

Jay, D. A., R. J. Uncles, J. Largier, W. R. Geyer, J. Vallino and W. R. Boynton (1997), A review of recent developments in estuarine scalar flux estimation, *Estuaries*, *20*, 262–280.

Jay, D. A., R. E. Flick, and T. Kukulka (2005), A long-term San Francisco Bay inflow record derived from tides: Defining the great flood of 1862, Abstract GC13B-1228 presented at 2005 Fall Meeting, AGU, San Francisco, Calif.

Jay, D. A., B. S. Giese, and C. R. Sherwood (1990), Energetics and sedimentary processes in the Columbia River estuary, *Prog. Oceanogr.*, *25*, 157–174.

Jay, D. A., K. Leffler, and S. Degens (2011), Long-term evolution of Columbia River tides, *J. Waterw. Port Coastal Ocean Eng.*, *137*, 182–191, doi:10.1061/(ASCE)WW.1943–5460.0000082.

Jay, D. A., R. J. Uncles, J. Largier, W. R. Geyer, J. Vallino, and W. R. Boynton (LMER Scalar Transport Working Group) (1997), A review of recent developments in estuarine scalar flux estimation, *Estuaries*, *20*, 262–280.

Kaiser, J. F. (1974), Nonrecursive digital filter design using the I0- sinh window function, paper presented at IEEE Symposium Circuits and Systems, Inst. of Electr. and Electron. Eng., San Francisco, Calif.

Kawanisi, K., M. Razaz, A. Kaneko, and S. Watanabe (2010), Long-term measurement of stream flow and salinity in a tidal river by the use of the fluvial acoustic tomography system, *J. Hydrol.*, *380*(1–2), 74–81.

Kimmerer, W. J. (2002), Physical, biological, and management responses to variable freshwater flow into the San Francisco estuary, *Estuaries*, *25*(6B), 1275–1290.

Kisi, O., and M. Cimen (2011), A wavelet-support vector machine conjunction model for monthly streamflow forecasting, *J. Hydrol.*, *399*, 132–140.

Knowles, N. (2002), Natural and management influences on freshwater inflows and salinity in the San Francisco Estuary at monthly to interannual scales, *Water Resour. Res.*, *38*(12), 1289, doi:10.1029/2001WR000360.

Kukulka, T., and D. A. Jay (2003a), Impacts of Columbia River discharges on salmonid habitat: 1. A nonstationary fluvial tidal model, *J. Geophys. Res.*, *108*(C9), 3293, doi:10.1029/2002JC001382.

Kukulka, T., and D. A. Jay (2003b), Impacts of Columbia River discharges on salmonid habitat: 2. Change in shallow-water habitat, *J. Geophys. Res.*, *108*(C9), 3294, doi:10.1029/2003JC001829.

Laize, C. L. R., and D. M. Hannah (2010), Modification of climate-river flow associations by basin properties, *J. Hydrol.*, *389*, 186–204, doi:10.1016/j.jhydrol.2010.05.048.

LeBlond, P. H. (1978), On tidal propagation in shallow rivers, *J. Geophys. Res.*, *83*, 4717–4721.

Leffler, K. E., and D. A. Jay (2009), Enhancing tidal harmonic analysis: Robust (hybrid L^1/L^2) solutions, *Cont. Shelf Res.*, *29*, 78–88.

Leung, L. R., Y. Qian, X. D. Bian, W. M. Washington, J. G. Han, and J. O. Roads (2004), Mid-century ensemble regional climate change scenarios for the western United States, *Clim. Change*, *62*, 75–113.

Logan, T. M. (1864), Contributions to the physics, hygiene and thermology of the Sacramento River, *Pac. Med. Surg. J.*, *7*, 145–151.

Loitzenbauer, E., and C. A. B. Mendes (2012), Salinity dynamics as a tool for water resources management in coastal zones: An application in the Tramandaí River basin, southern Brazil, *Ocean Coastal Manage.*, *55*, 52–62, doi:10.1016/j.ocecoaman.2011.10.011.

MacCready, P. (2011), Calculating estuarine exchange flow using isohaline coordinates*, *J. Phys. Oceanogr.*, *41*, 1116–1124, doi:10.1175/2011JPO4517.1.

Madsen, H., and C. Skotner (2005), Adaptive state updating in real-time river flow forecasting—A combined filtering and error forecasting procedure, *J. Hydrol.*, *308*, 302–312.

Monismith, S. G., W. Kimmerer, J. R. Burau, and M. T. Stacey (2002), Structure and flow-induced variability of the subtidal salinity field in Northern San Francisco Bay, *J. Phys. Oceanogr.*, *32*, 3003–3019, doi:10.1175/1520-0485(2002)032.

Mooney, C. Z. (1997), *Monte Carlo Simulation*, Sage Univ. Pap. Ser. Quan. Appl. Soc. Sci., 07–116, Sage Publication Inc., Thousand Oaks, Calif., doi:10.4135/9781412985116.

Nichols, F. H., J. E. Cloern, S. N. Luoma, and D. H. Peterson (1986), The modification of an estuary, *Science*, *231*, 567–573.

Oki, T., K. Musiake, H. Matsuyama, and K. Masuda (1995), Global atmospheric water balance and runoff from large river basins, *Hydrol. Processes*, *9*, 655–678, doi:10.1002/hyp.3360090513.

Palma, W., R. Escribano, and S. A. Rosales (2006), Modeling study of seasonal and inter-annual variability of circulation in the coastal upwelling site of the El Loa River off northern Chile, *Estuarine Coastal Shelf Sci.*, *67*, 93–107.

Parker, B. B. (1991), The relative importance of the various nonlinear mechanisms in a wide range of tidal interactions, in *Progress in Tidal Hydrodynamics*, edited by B. B. Parker, pp. 237–268, John Wiley, New York.

Parker, B. B. (2007), Tidal analysis and prediction, *NOAA Spec. Publ. NOS CO-OPS 3*, Silver Spring, Md.

Pawlowicz, R., B. Beardsley, and S. Lentz (2002), Classical tidal harmonics analysis including error estimates in MATLAB using T-TIDE, *Comput. Geosci.*, *28*, 929–937.

Peng, M., L. Xie, and L. J. Pietrafesa (2004), A numerical study of storm surge and inundation in the Croatan-Albemarle-Pamlico estuary system, *Estuarine Coastal Shelf Sci.*, *59*, 121–137.

Prandle, D. (1985), On salinity regimes and the vertical structure of residual flows in narrow tidal estuaries, *Estuarine Coastal Shelf Sci.*, *20*, 615–635.

Prandle, D. (2000), Operational oceanography—A view ahead, *Coastal Eng.*, *41*, 353–359.

Prandle, D. (2004), How tides and river flows determine estuarine bathymetries, *Prog. Oceanogr.*, *61*, 1–26.

Sassi, M. G., A. J. F. Hoitink, B. Vermeulen, and Hidayat (2011a), Discharge estimation from H-ADCP measurements in a tidal river subject to sidewall effects and a mobile bed, *Water Resour. Res.*, *47*, W06504, doi:10.1029/2010WR009972.

Sassi, M. G., A. Hoitink, B. de Brye, B. Vermeulen, and E. Deleersnijder (2011b), Tidal impact on the division of river discharge over distributary channels in the Mahakam Delta, *Ocean Dyn.*, *61*, 2211–2228, doi:10.1007/s10236-011-0473-9.

Savitzky, A., and M. J. E. Golay (1964), Smoothing and differentiation of data by simplified least squares procedures, *Anal. Chem.*, *36*(2), 1627–1639.

Schoellhamer, D. H., T. E. Mumley, and J. E. Leatherbarrow (2007), Suspended sediment and sediment-associated contaminants in San Francisco Bay, *Environ. Res.*, *105*, 119–131.

Smith, R. (2002), Historical Golden Gate tidal series, *NOAA Tech. Rep. NOS CO-OPS 035*, U.S. Department of Commerce, Washington, D. C.

Syvitski, J. P. M., S. D. Peckham, R. Hilberman, and T. Mulder (2003), Predicting the terrestrial flux of sediment to the global ocean: A planetary perspective, *J. Sediment. Geol.*, *162*, 5–24, doi:10.1016/S0037–0738(03)00232-X.

Talke, S. A., and D. A. Jay (2013), Nineteenth century Pacific and North American tidal data: Lost or just forgotten?, *J. Coastal Res.*, doi:10.2112/JCOASTRES-D-12-00181.1.

Taylor, J. R. (1997), *An Introduction to Error Analysis: The Study of Uncertainty in Physical Measurements*, 2nd ed., p. 325, Univ. Sci. Books, Sausalito, Calif.

Uncles, R. J., and D. H. Peterson (1996), The long-term salinity field in San Francisco Bay, *Cont. Shelf Res.*, *16*(15), 2005–2039.

Wang, W. C., K. W. Chau, C. T. Cheng, and L. Qiu (2009), A comparison of performance of several artificial intelligence methods for forecasting monthly discharge time series, *J. Hydrol.*, *374*, 294–306.

Woodworth, P. L. (2010), A survey of recent changes in the main components of the ocean tide, *Cont. Shelf Res.*, *30*(15), 1680–1691, doi:10.1016/j.csr.2010.07.002.